

Multi-Lepton Signatures of the Triplet Like Charged Higgs at the LHC

Priyotosh Bandyopadhyay^{a,b,1}, Katri Huitu^{a,2} and Aslı Sabancı Keçeli^{a,3}

^a*Department of Physics, and Helsinki Institute of Physics,*

P.O.Box 64 (Gustaf Hällströmin katu 2), FIN-00014 University of Helsinki, Finland

^b*Dipartimento di Matematica e Fisica "Ennio De Giorgi", Università del Salento and INFN, Via Arnesano, 73100, Lecce, Italy*

Email: ¹priyotosh.bandyopadhyay@helsinki.fi,

priyotosh.bandyopadhyay@le.infn.it, ²katri.huitu@helsinki.fi,

³asli.sabanci@helsinki.fi

ABSTRACT: We study multi-lepton signatures of the triplet like charged Higgs at the LHC in the context of $Y = 0$ triplet extended supersymmetric model (TESSM). In TESSM the $h_i^\pm W^\mp Z$ coupling appears at tree level when the triplet vacuum expectation value is nonzero, and because of the coupling the charged Higgs decay channels as well as the production channels can dramatically change at the LHC. We show that for the triplet dominated charged Higgs the main production channels are no longer through the top decay or gg and gb fusions since these are very suppressed due to the lack of triplet-SM fermion coupling. In the numerical analysis, we consider also other possible production channels some of which have additional contributions from the diagrams containing $h_i^\pm W^\mp Z$ vertex. We investigate the decay channels of a triplet like light charged Higgs ($m_{h_i^\pm} \leq 200$ GeV) and show that depending on the triplet component, the charged Higgs can substantially decay to $W^\pm Z$. We further examine the $3l$, $4l$, $5l$ multi-lepton signatures of the triplet like charged Higgs by considering four different benchmark points for which we perform PYTHIA level simulation using FastJet for jet formation at the LHC with 14 TeV. We found that for favorable parameters the earliest discovery with 5σ signal significance can appear with early data of 72 fb^{-1} of integrated luminosity. We also present the invariant mass distribution M_{ljj} for $(\geq 3l) + (\cancel{p}_T \geq 30 \text{ GeV})$ and $(\geq 3l) + (\geq 2j) + (\cancel{p}_T \geq 30 \text{ GeV})$ and show that in addition to the charged Higgs mass peak, an edge that carries information about heavy intermediate neutral Higgs bosons arises at the end of the mass distribution.

KEYWORDS: [Higgs](#), [Triplet Higgs](#), [Supersymmetry](#), [LHC](#).

Contents

1. Introduction	1
2. The Model	3
2.1 The Higgs Sector of the TESSM	5
3. The Charged Higgs Phenomenology	6
3.1 Charged Higgs Decay Channels	9
3.2 Charged Higgs Production Channels at the LHC	10
4. Benchmark points and final states	12
5. Collider simulation	16
5.1 3ℓ final states	17
5.2 4ℓ final states	19
5.3 5ℓ final states	20
6. Mass distributions	21
7. Conclusions	23

1. Introduction

The discovery of the Higgs boson [1,2] is a very important step toward understanding the nature of the electroweak symmetry breaking (EWSB) and its underlying model. Though the experimental results for Higgs production and decay channels are in very good agreement with the Standard Model (SM) predictions [3–12] there is still room for models beyond the SM which contain more than one Higgs boson in the particle spectrum. Such models are motivated by the problems of the SM such as unnaturalness of the Higgs mass, the lack of neutrino masses and a dark matter candidate.

The common feature of any extended Higgs sector possessing more than one Higgs doublet is to contain at least one charged Higgs pair along with the neutral Higgs bosons. Even though the discovery of a charged Higgs would be a clear evidence of a nonstandard

Higgs model, the subsequent analysis of the properties of charged Higgs is needed to reveal the structure as well as the symmetries of the Higgs sector.

The most studied possibility is to have only one charged Higgs boson pair (h^\pm) in the spectrum where the SM Higgs sector is extended by adding an extra Higgs doublet with or without supersymmetry (for reviews see *e.g.* Refs. [13] and [14]). In multi-doublet models, the charged Higgs can couple to the SM fermions and the main charged Higgs decay channels are tb and/or $\tau\nu_\tau$ depending on the mass of h^\pm [14, 15]. At the LHC, the light charged Higgs boson ($m_{h^\pm} \leq m_t - m_b$) is mainly produced by the top decay through $pp \rightarrow t\bar{t}$, $t \rightarrow h^\pm b$ [16, 17] whereas $gg \rightarrow tbh^\pm$ and $gb \rightarrow th^\pm$ channels become the dominant production channels for the heavy charged Higgs [18–22].

Besides the models with several Higgs doublets, the charged Higgs can be originated from the models comprising higher representations of Higgs fields such as triplets. In particular, the triplet models with non-zero triplet vacuum expectation value (vev) contains a tree level $h^\pm ZW^\mp$ coupling as a consequence of the custodial $SU(2)_c$ symmetry breaking. The appearance of this coupling at tree level is important for identifying the triplet’s impact in the charged Higgs since $h^\pm ZW^\mp$ coupling is induced at loop-level in the models with only Higgs doublets [23–26]. Thus this vertex opens up a new decay channel $h^\pm \rightarrow ZW^\mp$ as well as the charged Higgs production channel through the vector boson fusion.

To investigate the phenomenology of this coupling at LHC, we consider here the triplet extended supersymmetric model (TESSM) where the MSSM field content is extended by adding a $Y = 0$ triplet chiral superfield. After the Higgs discovery, this model has become an attractive alternative to the MSSM. The reason for this is that to accommodate a 125 GeV Higgs boson, in the MSSM large radiative corrections obtained via a large mixing between third generation squarks and/or very heavy stop masses [27] are needed. However, such a heavy spectrum results in a severe fine-tuning $\lesssim 1\%$ [28, 29]. Recently, it has been shown [32] that the fine-tuning can be reduced significantly when the TESSM is considered, since the extended Higgs sector can generate additional tree level contributions to the light Higgs mass so that sizable quantum corrections are no longer needed [30–32]. For the experimentally viable parameter regions of the model it is also possible to obtain an enhancement or a suppression in the Higgs decay to diphoton rate [32–35].

The other important feature of the TESSM is that the three charged Higgs pairs in the model can have different collider signatures compared to the charged Higgses originated from the Higgs doublets. For the triplet dominated charged Higgses, the production through the top decay or gg/gb fusions are no longer the most important channels at the LHC since triplet does not directly couple to the SM fermions. Though the charged Higgs sector of the TESSM has been partly studied in the literature [36, 37], all the possible

production/decay channels have to be investigated to understand the possibility to observe a triplet-like charged Higgs at the LHC. In this spirit, this study is dedicated to examine the possible decay and the production channels for the charged Higgses where the impact of $h^\pm ZW^\mp$ vertex is not negligible. During the analysis, we take into account the possible charged Higgs production channels such as the pair production $h_i^\pm h_j^\pm$, the associated gauge boson production $h_i^\pm Z$, $h_i^\pm W^\mp$ and the associated neutral Higgs production $h_i^\pm h_j$, $h_i^\pm A_j$, along with the gg and gb fusions.

Recent limits on the light charged Higgs at the LHC for 2HDM and MSSM have been obtained by considering $pp \rightarrow t\bar{t}$ with $t \rightarrow h^\pm b$ production channel and charged Higgs decay to $\tau\nu_\tau$ mode. The mass exclusion limits for the light charged Higgs have been attained by using $\mathcal{B}(t \rightarrow bh^\pm) \times \mathcal{B}(h^\pm \rightarrow \tau\nu)$ whereas for heavier charged Higgs bounds have been given for the effective production cross-section [38]. Certainly for the models with non-standard decays of the light charged Higgs, the present mass bounds are less tight and many regions of light charged Higgs can be still allowed by the data [39]. In this article we select four benchmark points to study and probe the triplet like charged Higgs ($m_{h_i^\pm} \sim 200$ GeV). We select our parameter points such that the triplet nature in the lightest charged Higgs allows ZW^\pm decay which can be as strong as tb and $\tau\nu_\tau$ modes when it is kinematically possible. A Pythia-Fastjet level simulation is carried out by taking care of dominant SM backgrounds. We analyse the signal in multi-lepton final states, i.e., with 3ℓ , 4ℓ , 5ℓ along with τ and b -jets. The requirements of multi-lepton and jets reduce the background substantially and earliest discovery hint can come with $\gtrsim 72$ fb $^{-1}$ of integrated luminosity.

The rest of the paper is organized as follows. In the next Section, we briefly review the model focusing especially on the Higgs sector where we give the effective formula describing the radiative corrections to the neutral Higgs masses. In Section 3, we investigate the features of the charged Higgses and especially focus on the tree level $h_i^\pm ZW^\pm$ coupling. We construct three different scenarios to show the impact of $h_i^\pm \rightarrow ZW^\pm$ decay on the branching ratio of the lightest charged Higgs. Then we discuss possible channels that can contribute to the charged Higgs production at the LHC. In Section 4, we introduce four different benchmark points with corresponding charged Higgs production cross-sections. In Section 5 we perform the collider simulations and discuss different final states. In Sections 6 and 7, we give our final remarks and conclusion.

2. The Model

In TESSM, the field content of the MSSM is enlarged by introducing an $SU(2)$ complex Higgs triplet with zero hypercharge which can be represented as a 2x2 matrix

$$\mathbf{T} = \begin{pmatrix} \sqrt{\frac{1}{2}}T^0 & T_2^+ \\ T_1^- & -\sqrt{\frac{1}{2}}T^0 \end{pmatrix}. \quad (2.1)$$

Here T^0 is a complex neutral field, while T_1^- and T_2^+ are the charged Higgs fields. Note that $(T_1^-)^* \neq -T_2^+$. The superpotential of the Higgs sector of the model is given by

$$W = \lambda \hat{H}_d \cdot \hat{T} \hat{H}_u + \mu_D \hat{H}_d \cdot \hat{H}_u + \mu_T \text{Tr}(\hat{T} \hat{T}) + y_t \hat{U} \hat{H}_u \cdot \hat{Q} - y_b \hat{D} \hat{H}_d \cdot \hat{Q} - y_\tau \hat{E} \hat{H}_d \cdot \hat{L}, \quad (2.2)$$

where μ_D is the usual mixing parameter of the two Higgs doublets and μ_T is the mass parameter of the triplet. The triplet field T couples to the two Higgs doublets by a dimensionless coupling λ and the triplet-SM fermion couplings are absent. We neglect other than the third generation Yukawa couplings. Note that “ \cdot ” represents contraction with antisymmetric ϵ_{ij} where $\epsilon_{12} = -1$. The soft SUSY breaking potential of the Higgs sector V_S can be written by using the convention of the superpotential as

$$V_S = m_{H_d}^2 |H_d|^2 + m_{H_u}^2 |H_u|^2 + m_T^2 \text{Tr}(T^\dagger T) + [B_D \mu_D H_d \cdot H_u + B_T \mu_T \text{Tr}(TT) + A_\lambda \lambda H_d \cdot T H_u + y_t A_t \tilde{t}_R^* H_u \cdot \tilde{Q}_L - y_b A_b \tilde{b}_R^* H_d \cdot \tilde{Q}_L + \text{h.c.}]. \quad (2.3)$$

Here A_j ($j = \lambda, t, b$) are the soft trilinear parameters, B_D and B_T are the soft bilinear parameters, while m_i ($i = H_d, H_u, T$) represent the soft SUSY breaking masses. For simplicity we assume that there is no CP violation in the Higgs sector and all the parameters as well as the vacuum expectation values of the neutral Higgs fields (vevs) are chosen to be real. When these neutral fields acquire non-zero vevs, denoted by

$$\langle H_u^0 \rangle = \frac{v_u}{\sqrt{2}}, \quad \langle H_d^0 \rangle = \frac{v_d}{\sqrt{2}}, \quad \langle T^0 \rangle = \frac{v_T}{\sqrt{2}}, \quad (2.4)$$

and $\tan \beta = v_u/v_d$, the electroweak symmetry is spontaneously broken and all fermions and gauge bosons gain masses. The W boson mass expression is altered by the triplet vev as $m_W^2 = g_2^2(v^2 + 4v_T^2)/4$, where $v^2 = v_u^2 + v_d^2$; whereas the Z boson mass expression remains unaffected. This non-zero triplet contribution to W mass leads to a deviation in the tree-level ρ parameter expression,

$$\rho = 1 + 4v_T^2/v^2. \quad (2.5)$$

Thus the triplet vev is strongly constrained by the global fit on the ρ parameter measurement [40],

$$\rho = 1.0004^{+0.0003}_{-0.0004} \quad (2.6)$$

which implies $v_T \leq 5$ GeV. Such a stringent constraint on the triplet vev prevents the triplet extension from generating μ_D term effectively as a solution for μ problem of the MSSM.

This is why we write the μ_D term and the triplet-doublet interaction term separately in the superpotential. However, small v_T can still generate deviations in the Higgs sector as we show in the following Sections. In the numerical analysis of this paper we use a fixed value $v_T = 3\sqrt{2}$ GeV for the triplet vev.

2.1 The Higgs Sector of the TESSM

After the electroweak symmetry breaking the physical particle spectrum of the TESSM Higgs sector comprises three CP-even ($h_{1,2,3}$), two CP-odd ($A_{1,2}$) and three charged Higgs bosons ($h_{1,2,3}^\pm$). In our notation, h_1 corresponds to the lightest Higgs boson of the model whereas the others are generally much heavier. It was shown in Ref. [32, 33] that it is possible to obtain the lightest Higgs boson with a mass up to 125 GeV even at tree level when λ is so large that the model is in the non-perturbative regime at the high scales. As long as we demand perturbativity of the model, for a 125 GeV Higgs one needs radiative corrections to the neutral Higgs sector which, however, are not necessarily as large as those in the MSSM [30–32, 34, 37]. The additional contributions to Higgs mass therefore decreases the required limits on the third generation squarks significantly [30] and the corresponding fine-tuning can be greatly reduced as compared to values attainable in MSSM [32]. The one-loop radiative corrections to the Higgs potential can be calculated using the effective potential approach [41]

$$\Delta V = \frac{1}{64\pi^2} \text{Str} \left[\mathcal{M}^4 \left(\ln \frac{\mathcal{M}^2}{\Lambda^2} - \frac{3}{2} \right) \right]. \quad (2.7)$$

Here Λ is the renormalization scale and \mathcal{M} represents the field dependent mass matrices that can be found in Ref. [32]. In the current study, we consider the radiative corrections coming both from the colored sector and the electroweak sector since it is known that for TESSM the neutralino and chargino corrections can have crucial impact on the lightest Higgs mass [30, 32, 33]. For the numerical calculations, we use an effective formula for the 1-loop contributions to the CP even scalar mass matrix [32, 33]

$$\begin{aligned} (\Delta \mathcal{M}_{h^0}^2)_{ij} &= \left. \frac{\partial^2 \Delta V(a)}{\partial a_i \partial a_j} \right|_{\text{vev}} - \frac{\delta_{ij}}{\langle a_i \rangle} \left. \frac{\partial \Delta V(a)}{\partial a_i} \right|_{\text{vev}} \quad (2.8) \\ &= \sum_k \frac{1}{32\pi^2} \frac{\partial m_k^2}{\partial a_i} \frac{\partial m_k^2}{\partial a_j} \ln \frac{m_k^2}{\Lambda^2} \Big|_{\text{vev}} + \sum_k \frac{1}{32\pi^2} m_k^2 \frac{\partial^2 m_k^2}{\partial a_i \partial a_j} \left(\ln \frac{m_k^2}{\Lambda^2} - 1 \right) \Big|_{\text{vev}} \\ &\quad - \sum_k \frac{1}{32\pi^2} m_k^2 \frac{\delta_{ij}}{\langle a_i \rangle} \frac{\partial m_k^2}{\partial a_i} \left(\ln \frac{m_k^2}{\Lambda^2} - 1 \right) \Big|_{\text{vev}}, \quad i, j = u, d, T. \quad (2.9) \end{aligned}$$

Here m_k^2 is the set of eigenvalues of the field dependent mass matrices given in Ref. [32] where the real components (a_j) of the neutral Higgs fields are defined as $H_u^0 =$

$1/\sqrt{2}(a_u + ib_u)$, $H_d^0 = 1/\sqrt{2}(a_d + ib_d)$ and $T^0 = 1/\sqrt{2}(a_T + ib_T)$. For simplicity we drop the supertrace expressions in Eq. (2.9) but for each particle, the supertrace coefficient should be taken into account.

In the rest of the paper we particularly focus on the charged Higgs sector of the model. The charged Higgs in TESSM has been partly investigated in the literature earlier [36,37]. Further studies are needed regarding the mass spectrum and the LHC signatures of the charged Higgses to pin down the structure and symmetries of the underlying Higgs sector. In this spirit, we perform a scan for the viable points containing one ~ 125 GeV neutral Higgs in the spectrum and discuss the features of the charged Higgs sector of TESSM in the next section.

3. The Charged Higgs Phenomenology

The charged Higgs boson is a clear indication of a non-standard Higgs sector since SM predicts only one neutral scalar boson in the particle spectrum. The existence of at least one charged Higgs is predicted by many models with different multiplet structure and probing the properties of charged Higgs can differentiate between the models. For this purpose, we first investigate the mass hierarchy among the Higgs bosons of TESSM to distinguish the model from the ones containing only Higgs doublets in their field contents. To present the properties of the TESSM Higgs sector, we perform a scan for which the parameter ranges are defined as:

$$1 \leq \tan \beta \leq 30, \quad |\lambda| \leq 1, \quad 0 \leq |\mu_D, \mu_T| \leq 2 \text{ TeV}, \quad 100 \text{ GeV} \leq |M_1, M_2| \leq 1 \text{ TeV},$$

$$0 \leq |A_t, A_b, A_\lambda, B_D, B_T| \leq 2 \text{ TeV}, \quad 500 \text{ GeV} \leq m_Q, m_{\tilde{t}}, m_{\tilde{b}} \leq 2 \text{ TeV} \quad (3.1)$$

where $m_Q, m_{\tilde{t}}, m_{\tilde{b}}$ are the left- and right-handed squark soft masses and M_i ($i=1,2$) are the soft gaugino masses. In this parameter scan, we collect the random parameter points that respect the following constraints

$$124 \leq m_{h_1^0} \leq 127 \text{ GeV} ; \quad m_{A_{1,2}}, m_{\chi_{1,2,3,4,5}^0} \geq 65 \text{ GeV} ;$$

$$m_{\chi_{1,2,3}^\pm} \geq 104 \text{ GeV} ; \quad m_{\tilde{t}_{1,2}}, m_{\tilde{b}_{1,2}} > 600 \text{ GeV} . \quad (3.2)$$

Here our bound for neutralinos is stronger than the experimental one in order to avoid the constraints from the invisible decays of the lightest Higgs boson. Such decays are relevant for the dark matter studies [35]. In Fig. 1a (b) we display the mass hierarchy between the lightest charged Higgs boson and the heavier CP even Higgs boson h_2 (CP odd A_1) for the viable points respecting the aforementioned constraints. Unlike in the case of MSSM, often the lightest charged Higgs is non-degenerate in mass with CP odd

and heavy CP even Higgs bosons. Such non-degeneracy has a great importance since on-shell decays like $h_2(A_1) \rightarrow h_1^\pm W^\pm$ are now kinematically possible and can give significant contribution to the charged Higgs production cross-section. We also observe that for the obtained parameter points, the heaviest CP odd (A_2) and CP even (h_3) Higgs bosons have mass $\gtrsim 500$ GeV. Their negligible contributions to the total production cross-section are not considered during the collider simulations.

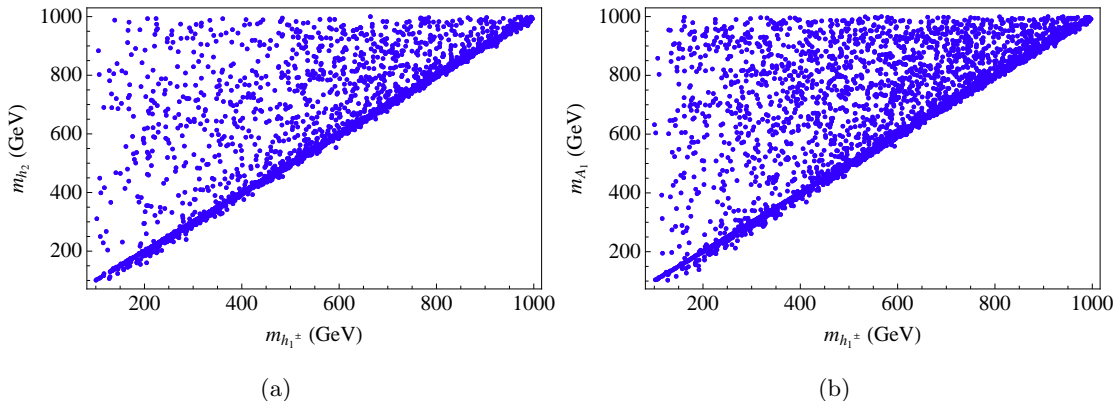


Figure 1: The mass hierarchy between the lightest charged Higgs boson and (a) the heavier CP even Higgs h_2 (b) the CP odd Higgs boson A_1 .

In addition to non-degeneracy, the charged Higgs couplings to SM fermions and gauge bosons must be revisited to understand the triplet impact. It is known that in two Higgs doublet models (with or without supersymmetry), $h^\pm ZW^\mp$ coupling can be induced only at loop order since the custodial $SU(2)_c$ symmetry prohibits the tree level interaction. However, for $Y = 0, \pm 2$ triplet extended models, the custodial symmetry is broken by the triplet vev that allows non-zero $h_i^\pm ZW^\mp$ coupling at tree level. This coupling has a great importance since its verification could indicate the evidence of higher multiplet structure in the electroweak sector. For the $Y = 0$ triplet extended model this coupling can be written as

$$g_{h_i^\pm W^\mp Z} = -\frac{1}{2}ig_2 \left[g_1 \sin \theta_w (v_u R_{(i+1)1} - v_d R_{(i+1)2}) + \sqrt{2}g_2 v_T \cos \theta_w (R_{(i+1)3} + R_{(i+1)4}) \right], \quad (3.3)$$

where g_1 and g_2 are the electroweak gauge couplings and θ_w is the Weinberg angle. R_{ij} are the rotation matrix entries of charged Higgs sector and the physical charged Higgses are related with the charged fields as

$$\begin{pmatrix} G^+ \\ h_1^+ \\ h_2^+ \\ h_3^+ \end{pmatrix} = \begin{pmatrix} R_{11} & R_{12} & R_{13} & R_{14} \\ R_{21} & R_{22} & R_{23} & R_{24} \\ R_{31} & R_{32} & R_{33} & R_{34} \\ R_{41} & R_{42} & R_{43} & R_{44} \end{pmatrix} \begin{pmatrix} H_u^+ \\ H_d^{-*} \\ T_2^+ \\ T_1^{-*} \end{pmatrix}. \quad (3.4)$$

During the investigation of the $h_i^\pm W^\mp Z$ coupling strength, the numerically calculated 4×4 rotation matrix entries require special attention. When one of the R_{ij} entries is set to a value, the other entries must be chosen carefully so as to respect the electromagnetic gauge symmetry that ensures $h_i^\pm W^\pm \gamma$ coupling to be zero.

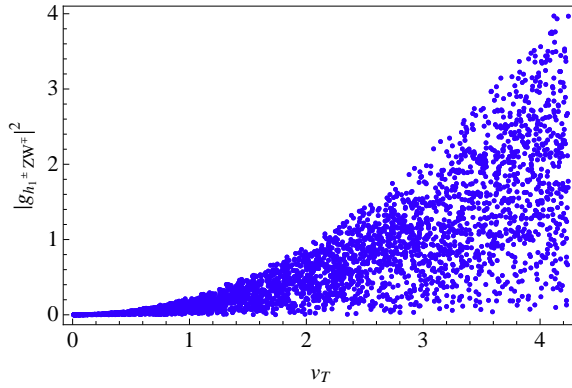


Figure 2: $|g_{Zh_1^\pm W^\mp}|^2$ as a function of v_T : For $v_T = 0$ the coupling vanishes due to the $U(1)_{em}$ gauge invariance.

In order to see the strength of the coupling we perform another scan where we consider $1 \leq \tan \beta \leq 30$ and display the coupling strength $|g_{Zh_1^\pm W^\mp}|^2$ as a function of v_T in Fig. 2. When v_T is non-zero the first term¹ contributes along with the second term and according to the doublet-triplet content in the charged Higgs, the coupling can be suppressed or enhanced. However, when v_T is zero the coupling vanishes since expressions in the parenthesis in the first part of the coupling must cancel each other not to lead to the tree level $h_i^\pm W^\mp \gamma$ coupling that breaks the electromagnetic gauge invariance. In other words, $h_i^\pm ZW^\pm$ can survive only for non-zero triplet vacuum v_T . Similar situation arises when the triplet is completely decoupled from the doublet sector. For the doublet like lightest charged Higgs the second term in the coupling again drops and the two terms in the first part cancels exactly like in the case of MSSM. To understand the impact of this tree level coupling on the charged Higgs decays, the next section is devoted to the study on the light charged Higgs branching ratios where we construct different scenarios to reveal the triplet effect on the decay channels.

¹The first term was not considered in Ref. [36].

3.1 Charged Higgs Decay Channels

We now discuss the decay of the lightest charged Higgs boson in the low mass region $150 < m_{h_1^\pm} \lesssim 200$ GeV. To show the impact of the triplet nature, we construct three scenarios where charged Higgs has the different percentage of triplet component. During the numerical analysis, we set $R_{23} = 0.3$ in the $h_1^\pm ZW^\mp$ coupling and we determine the other R_{ij} parameters ensuring that the $h_1^\pm W^\mp \gamma$ coupling is zero at tree level. For the numerical analysis we select the following scenarios:

- *Scenario I (Sc I)*: The rest of the R_{ij} elements in the $h_1^\pm ZW^\mp$ coupling are arranged in such a way that the triplet component in the lightest charged Higgs is 90%.
- *Scenario II (Sc II)*: The rest of the R_{ij} elements are chosen for the lightest charged Higgs to comprise 1% doublet and 99% triplet.
- *Scenario III (Sc III)*: The charged Higgs is composed of 0.1% doublet and 99.9% triplet.

To determine the branching ratios of the lightest charged Higgs in TESSM we employ SARAH [46, 47] program to generate the model files for CalcHep [48] and we display the results in Fig.3. For this analysis we choose $\tan\beta = 5$ and 30 to investigate the low and high $\tan\beta$ behaviors for all scenarios. When the doublet component of the lightest charged Higgs is 10% (Scenario I) for $\tan\beta = 5$, $\mathcal{B}r(h_1^\pm \rightarrow ZW^\pm)$ can reach up to 25% for $m_h^\pm \sim 175$ GeV (See Fig. 3a). However, as soon as tb channel is kinematically possible the branching ratio to ZW^\pm drops to 10%. For $\tan\beta = 30$ for $m_{h_1^\pm} \leq m_t + m_b$ region the dominant decay channel is $\tau\nu_\tau$ and ZW^\pm channel is very suppressed. For a heavier charged Higgs mass, tb channel becomes as important as $\tau\nu_\tau$ whereas the ZW^\pm channel has an insignificant branching.

This behavior changes completely in the case of Sc II. When the triplet component increases in the lightest charged Higgs, its coupling to fermions diminishes since triplet does not couple to the SM fermions directly and thus the fermionic branching ratios drop significantly. For $\tan\beta = 5$, the branching ratio to ZW^\pm increases dramatically and it can be as high as 80% (See Fig. 3b). When tb channel is open the ZW^\pm branching ratios drops to $\sim 30\%$ but it still much larger than $\tau\nu_\tau$ branching ratios.

In Sc III, the lightest charged Higgs is almost triplet and ZW^\pm channel becomes the most dominant decay channel even after tb decay is kinematically possible. The branching can be as high as 100% for $\tan\beta = 5$ and it drops to $\sim 50\%$ for $m_{h_1^\pm} = 200$ GeV (Fig. 3c). For $\tan\beta = 30$ the situation is similar except that the branching ratio can reach up to $\sim 90\%$ for the mass region $170 \leq m_{h_1^\pm} \leq 180$ GeV.

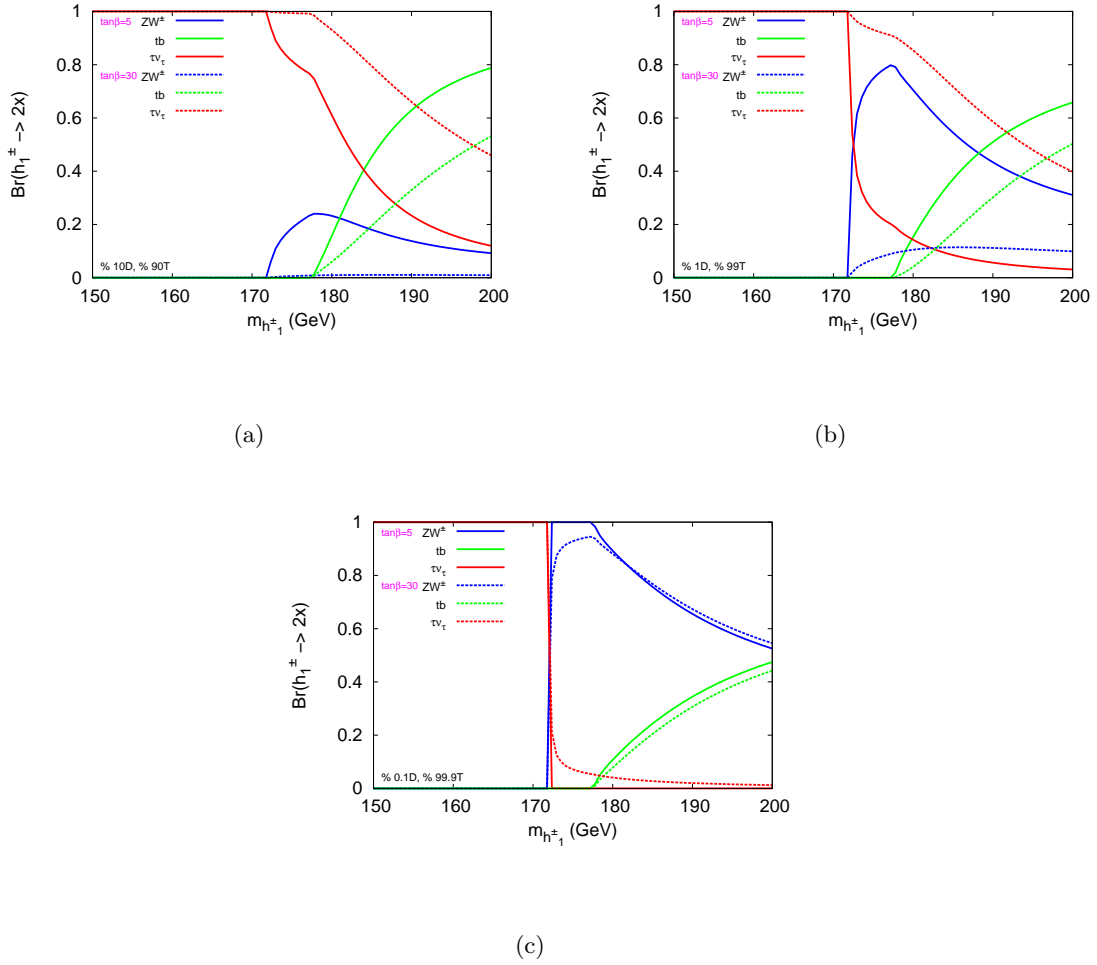


Figure 3: The branching ratios of the lightest charged Higgs for (a) Scenario I (b) Scenario II and (c) Scenario III.

Next we focus on triplet effect on the charged Higgs production channels at LHC and we discriminate the dominant charged Higgs production channels for TESSM from the ones in the isospin doublet models.

3.2 Charged Higgs Production Channels at the LHC

The production channels for the charged Higgses depend strongly on the model under consideration. When the model has only Higgs doublets (*e.g.* 2HDM, MSSM), the main production channel of the charged Higgs with mass $m_{h_i^\pm} \leq m_t - m_b$ is $pp \rightarrow t\bar{t}$ and the subsequent top quark decay to b and the charged Higgs boson. For $m_{h_i^\pm} \geq m_t + m_b$ the dominant channels are the associated production with a top quark in gb and gg fusions [17–20]. The $q\bar{q}$ annihilation also contributes non-negligibly to the latter case. However $gg \rightarrow tbh_i^\pm$ and $gb(g\bar{b}) \rightarrow th_i^-(\bar{t}h_i^+)$ channels are expected to be suppressed in TESSM

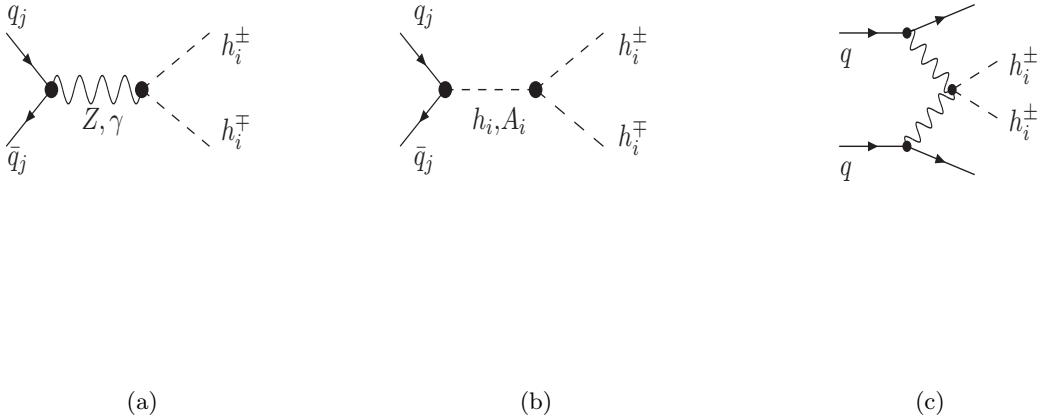


Figure 5: Some example diagrams for the charged Higgs pair production at LHC for TESSM.

the TESSM Higgs sector contains more neutral Higgses than 2HDM or MSSM, and this affects the production cross-section in question. In Fig. 5 we show some example diagrams for the charged Higgs pair production mechanisms that can give significant contributions to the signals that we investigate in collider simulation section. The triplet nature of the neutral Higgses can also play an important role since the processes in Fig. 4e and Fig. 5b are expected to be suppressed for triplet like neutral Higgses. The analysis for determining the dominant production channel of the charged Higgs must be carried out carefully by investigating the nature of all Higgs bosons.

In the following section, we consider four benchmark points with the triplet percentages in the neutral and charged Higgses and we determine the dominant production mechanism of the lightest charged Higgs for each benchmark point and study the possible multi-lepton signatures at the LHC.

4. Benchmark points and final states

For the collider analysis we mainly consider phenomenology of the light charged Higgs with mass $m_{H^\pm} \sim 200$ GeV. The light charged Higgs scenario is very interesting for distinguishing the nature of the Higgs sector. The reason behind is that in the models containing two doublets and/or singlets such a light charged Higgs boson mainly decays to either tb or $\tau\nu$ whereas in models with SM-fermiophobic triplet such as TESSM these decays are expected to be suppressed. As discussed in the previous sections, for these models ZW^\pm decay channel can become as significant as the fermionic ones. To show the impact of the triplet nature on the decay and production channels of the charged Higgs here we consider four different benchmark points (BP's) with various doublet-triplet mixing in the Higgs

Benchmark	$\tan \beta$	m_{h_2}	m_{A_1}	$m_{h_1^\pm}$	Doublet	Doublet	Triplet
Points		(GeV)	(GeV)	(GeV)	% in h_2	% in A_1	% in h_1^\pm
BP1	8.63	182.898	610.91	182.942	1.34	99.967	98.88
BP2	4.89	216.94	451.453	216.41	0.2	$< 10^{-5}$	99.88
BP3	6.32	441.507	198.438	197.854	0.12	$< 10^{-5}$	99.99
BP4	7.23	362.843	184.706	183.637	0.78	0.006	99.98

Table 1: Benchmark points for a collider study consistent with the ~ 125 GeV Higgs mass where the h_2 , A_1 and h_1^\pm masses are calculated at tree level.

sector. During the analysis we focus on the low $\tan \beta$ region ($\tan \beta \leq 10$) which is favored by small fine-tuning [32]. In this region the tree level triplet contribution to the Higgs mass is maximized with large values of λ [32,33] so that as sizable loop corrections as in the case of MSSM are not needed.

Table 1 shows the benchmark points chosen for our collider study in the next section. For our purposes, we consider the benchmark points that contain the lightest neutral Higgs with a mass calculated at one loop level satisfying the range $124 \leq m_h \leq 127$ GeV. It is checked that all the benchmark points satisfy the experimental results for the Higgs decay rate to ZZ and WW within 2σ [42,43]. We also check that for all the benchmark points both heavy neutral Higgs bosons (h_2 and A_1) respect the CMS [44] and ATLAS [45] cross-section constraints at 2σ level. The lightest charged Higgs in all the four benchmark points has a substantial triplet component ($\gtrsim 99\%$) that enlarges the branching ratio of the ZW^\pm channel as seen in the section 3.1. We can see that either the lightest pseudo scalar A_1 (in BP3 and BP4) or the second lightest scalar h_2 (in BP1 and BP2) masses are nearly degenerate with the charged Higgs boson mass. The other heavier neutral Higgs bosons h_2 (in BP3 and BP4) and A_1 (in BP1 and BP2) can decay to the lightest charged Higgs boson (h_1^\pm), unlike the cases of 2HDM and MSSM, where the heavier neutral Higgses (A, H) are almost degenerate with the charged Higgs boson in the spectrum. Thus for the studied benchmark points the decay modes are drastically different than in MSSM case with heavy Higgs bosons.

Table 2 presents the decay branching fraction for the second lightest CP-even scalar, h_2 , where dash lines show the kinematically forbidden decays. We can see that in the case of BP1, $W^\mp h_1^\pm$ channel is not open and h_2 mainly decays to $b\bar{b}$ due to its 1.34% doublet

h_2 Decay	Branching fractions(%)							
Modes	$W^\pm h_1^\mp$	$W^\pm W^\mp$	$A_1 Z$	ZZ	$h_1 h_1$	$b\bar{b}$	$t\bar{t}$	$\tau\bar{\tau}$
BP1	-	1.72	-	3.36	-	90.2	-	4.70
BP2	-	55.0	-	43.6	-	1.33	-	6.93×10^{-2}
BP3	69.2	12.1	2.1×10^{-9}	6.71	8.15	0.0121	3.81	6.24×10^{-4}
BP4	80.8	6.74	7.96×10^{-3}	3.97	5.01	3.08	0.201	0.160

Table 2: Decay branching fractions of h_2 for the benchmark points where the h_2 mass is calculated at tree level. The kinematically forbidden decays are marked with dashes.

A_1 Decay	Branching fractions (%)							
Modes	$W^\pm h_1^\mp$	$\chi_1^\pm \chi_1^\mp$	$h_1 Z$	$h_2 Z$	$\chi_1^0 \chi_1^0$	$b\bar{b}$	$t\bar{t}$	$\tau\bar{\tau}$
BP1	26.6	0.262	0.140	13.4	0.756	46.1	10.1	2.39
BP2	99.999	-	$< 10^{-7}$	$< 10^{-7}$	-	$< 10^{-3}$	$< 10^{-3}$	$< 10^{-4}$
BP3	-	-	9.42×10^{-5}	-	-	95.1	-	4.93
BP4	-	-	6.65×10^{-8}	-	-	95.1	-	4.94

Table 3: Decay branching fraction of A_1 for the benchmark points where A_1 mass calculated at tree level. The kinematically forbidden decays are marked with dashes.

component. For BP2, the $b\bar{b}$ channel is very suppressed since h_2 is mostly triplet so it decays mainly to gauge boson pairs ($W^\pm W^\mp$ and ZZ). For BP3 and BP4, $h_1^\pm W^\mp$ channel is kinematically open and it becomes the dominant decay channel due to the triplet nature of h_2 .

Next we consider the decay branching fractions of the pseudo-scalar boson, A_1 as given in Table 3. In the case of BP1, A_1 is mostly of doublet type and decays preferably to the fermionic final states, i.e., $b\bar{b}$, $t\bar{t}$ or $\tau\bar{\tau}$. In case of BP2 it is almost a triplet so that the A_1 dominantly decays to $W^\pm h_1^\mp$. In BP3 and BP4 A_1 is of triplet type, but due to the non-available phase space, it decays only into $b\bar{b}$ and $\tau\bar{\tau}$.

In Table 4 we show the decay branching fractions for the charged Higgs boson for each benchmark point. As seen in section 3.1, doublet content $\lesssim 1\%$ is enough to open the

h_1^\pm Decay	Branching fractions (%)			
Modes	ZW^\pm	h_1W^\pm	$t\bar{b}$	$\tau\bar{\nu}_\tau$
BP1	56.3	-	17.4	26.3
BP2	41.4	9.42	49.1	3.27×10^{-2}
BP3	59.4	-	40.2	0.44
BP4	38.7	9.72×10^{-2}	12.8	48.4

Table 4: Decay branching fraction of h_1^\pm for the benchmark points.

Benchmark Points	$\sigma_{h_1^\pm tb}$ fb	$\sigma_{h_1^\pm t}$ fb	$\sigma_{h_1^\pm h_1}$ fb	$\sigma_{h_1^\pm h_2}$ fb	$\sigma_{h_1^\pm A_1}$ fb	$\sigma_{h_1^\pm h_1^\mp}$ fb	$\sigma_{h_1^\pm W^\mp}$ fb	$\sigma_{h_1^\pm Z}$ fb
BP1	11.12	16.39	2.02	301.84	3×10^{-2}	151.9	225.504	0.64
BP2	3.8	5.4	0.39	162.1	3.9×10^{-2}	80.77	1.013	0.36
BP3	6.4×10^{-3}	8×10^{-3}	3×10^{-4}	5×10^{-2}	226.6	99.4	2.6×10^{-2}	0.27
BP4	1.6×10^{-3}	3×10^{-2}	11×10^{-4}	0.246	296.9	149.9	17.4	2.6×10^{-3}

Table 5: The important production cross-sections at NLO of four benchmark points at the LHC with ECM=14 TeV. The K factor is taken as $K=1.6$.

tb or $\tau\nu$ decay modes. In all four benchmark points we have substantial ZW^\pm as well as fermionic decay branching fractions. In the case of BP2 the decay mode h_1W^\pm becomes kinematically allowed.

Table 5 presents the cross-sections of the lightest charged Higgs production processes at the LHC. To calculate these cross-sections we obtained related vertices with proper doublet-triplet mixing from SARAH [46,47]. The vertex information and mass spectrum are then fed to CalcHEP [48] to calculate the production cross-sections with 14 TeV center of mass energy at the LHC where we use CTEQ6L parton distribution function (PDF) [53,54]. The renormalization/factorization scale in CalcHEP is set at $\sqrt{\hat{s}}$. A K -factor of 1.6 is taken for the NLO cross-section evolution [14]. In the numerical analysis we see that the cross-section for $h_1^+h_1^-$ is substantial for all our benchmark points. The $h_1^\pm h_2$ production cross-section is large for BP1 and BP2 where h_2 is degenerate in mass with h_1^\pm . The

production cross-section of $h_1^\pm A_1$ is large for BP3 and BP4 due to the light A_1 while the production cross-section for $h_1^\pm W^\mp$ is large only for BP1 and BP4 since doublet components in h_2 and A_1 (given in Table 1) enhance the contributions coming from the diagrams given in Fig. 4d-e. We also see that due to the large triplet part in the light h_1^\pm the production processes, i.e., $h_1^\pm t$ and $h_1^\pm tb$ fail to contribute as much as the other production processes in TESSM. Finally we observe that the production cross-sections of $h_1^\pm Z$ and $h_1^\pm h_1$ are negligible for our BP's and those cross-sections are not taken into account in the collider analysis.

5. Collider simulation

In this study, SARAH [46, 47] is used to generate the vertices for TESSM. The one-loop lightest neutral Higgs mass spectrum is generated by our self developed mathematica code. The vertex information and mass spectrum are then fed to CalcHEP [48] which generates the decay branching fractions, which we write in SLHA [51] format readable to PYTHIA. The events for the simulation were either generated by PYTHIA (version 6.4.5) [52] or CalcHEP [48] and later fed to PYTHIA for simulation.

For hadronic level simulation we have used Fastjet-3.0.3 [49] algorithm for the jet formation with the following criteria:

- The calorimeter coverage is $|\eta| < 4.5$.
- As we are looking for leptonic final states we demand hard jets, $p_{T,min}^{jet} = 20$ GeV and jets are ordered in p_T .
- Leptons ($\ell = e, \mu$) are selected with $p_T \geq 10$ GeV and $|\eta| \leq 2.5$.
- No jet should match with a hard lepton in the event.
- $\Delta R_{lj} \geq 0.4$ and $\Delta R_{ll} \geq 0.2$. Here $\Delta R_{ij} = \sqrt{\Delta\phi_{ij}^2 + \Delta\eta_{ij}^2}$ is the angle between particle i and particle j, where $\Delta\phi_{ij}$ is the difference of the azimuthal angle and $\Delta\eta_{ij}$ is the difference of the pseudo-rapidities.
- Since efficient identification of the leptons is crucial for our study, we required, on top of the above set of cuts, that hadronic activity within a cone of $\Delta R = 0.3$ between two isolated leptons should be $\leq 0.15 p_T^\ell$ GeV in the specified cone.

In Figure 6 we show the lepton multiplicity distribution for benchmark point 1 (BP1) coming from the dominant production processes, $h_1^\pm h_2$, $h_1^\pm W^\mp$ and $h_1^\pm h_1^\mp$. We see that there are sufficient number of events with more than 3ℓ which can kill many SM backgrounds and reduce substantially the others. In the following sections we demand $\geq 3\ell$

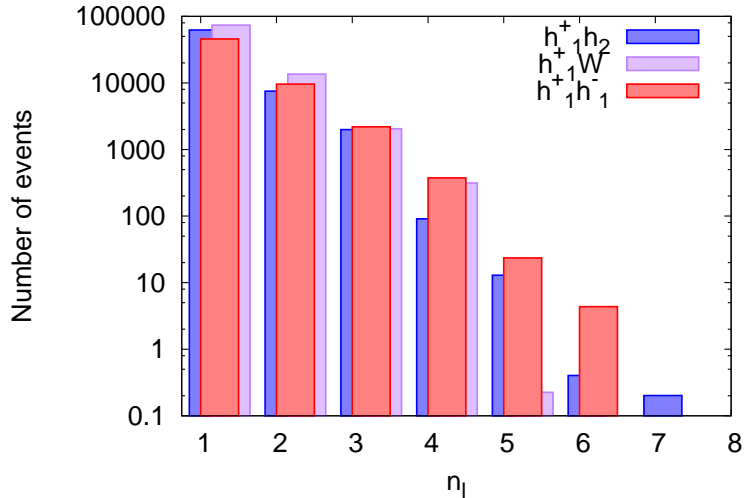


Figure 6: The lepton multiplicity distributions coming from the dominant production processes, $h_1^\pm h_2$, $h_1^\pm W^\mp$ and $h_1^\pm h_1^\mp$, respectively, for BP1 at the LHC at 1000 fb^{-1} of integrated luminosity.

also use different selection cuts to reduce the SM background further and investigate the minimum required luminosity to have the discovery at 5σ signal significance.

5.1 3ℓ final states

We can see from the dominant production processes that the charged Higgs, h_1^\pm , decays to ZW^\pm can give rise to 3ℓ final states. The other associated particles like h_2/A_1 , W^\pm and the other charged Higgs h_1^\pm (in case of the pair production) can contribute in the jet-final states through their hadronic decays. Keeping this in our mind and to kill the standard model backgrounds (SM) we look for $\geq 3\ell + (\geq 2 - \text{jet})$ final state. Out of these 3 leptons one pair is coming from the Z , so we also demand $|M_{\ell\ell} - M_Z| \leq 5 \text{ GeV}$. We choose our final state as $[\geq 3\ell (|M_{\ell\ell} - M_Z| \leq 5 \text{ GeV})] + \geq 2j + (\cancel{p}_T \geq 30 \text{ GeV})$ and the respective number of events for the benchmark points and the dominant SM backgrounds are listed in Table 6 at an integrated luminosity of 1000 fb^{-1} at the 14 TeV LHC. For the SM backgrounds we have considered productions of $t\bar{t}$, $t\bar{t}Z$, $t\bar{t}W^\pm$ and VV (which includes W^+W^- , $W^\pm Z$ and ZZ) of which $t\bar{t}$ and VV are the dominant ones. As the numbers are given for an integrated luminosity of 1000 fb^{-1} , all four benchmark points cross 5σ of signal significance; the highest is $\sim 19\sigma$ for BP1 and lowest is $\sim 9\sigma$ for BP4. The earliest 5σ signal significance comes at an integrated luminosity of 72 fb^{-1} for BP1. For BP4 we

have to wait for around 300 fb^{-1} of integrated luminosity.

Production processes	Benchmark Points				Backgrounds			
	BP1	BP2	BP3	BP4	$t\bar{t}$	$t\bar{t}Z$	$t\bar{t}W$	VV
$h_1^+ h_1^-$	809.72	469.11	659.09	480.10				
$h_1^\pm W^\mp$	645.55	0.00	0.00	25.97				
$h_1^\pm \phi$	903.04	834.23	716.21	581.56	2084.34	333.72	190.66	11043.99
$h_1^\pm t$	58.92	18.44	0.00	0.00				
$h_1^\pm tb$	53.23	17.54	0.00	0.00				
Total	2470.46	1339.31	1375.30	1087.63	13652.71			
Significance	18.64	10.66	11.22	8.96				

Table 6: Number of events after the selection cuts for $\geq 3\ell (|M_{\ell\ell} - M_Z| \leq 5 \text{ GeV}) + \geq 2j + (\cancel{p}_T \geq 30 \text{ GeV})$ final state for the benchmark points and backgrounds at an integrated luminosity of 1000 fb^{-1} at the LHC with $E_{cm} = 14 \text{ TeV}$. Here $h_1^\pm \phi$ includes contributions from both $h_1^\pm h_2$ and $h_1^\pm A_1$.

Next we focus on the possibility to tag the charged Higgs boson in association with a neutral Higgs, i.e., h_2 or/and A_1 . We can see from Table 2 and Table 3 that either of these two Higgses decays to $b\bar{b}$ substantially except in BP2. In the case of BP1 and BP2 it is mainly $h_1^\pm h_2$ that contributes due to lighter masses of h_2 and higher production rates (see Table 5). The situation is quite opposite in the case of BP3 and BP4 where $h_1^\pm A_1$ contributes instead of $h_1^\pm h_2$.

For the final state we demand $\geq 3\ell (|M_{\ell\ell} - M_Z| \leq 5 \text{ GeV}) + (\geq 2b - \text{jets}) + (\cancel{p}_T \geq 30 \text{ GeV})$, where we expect the two b jets mostly come from the neutral Higgses. The charged Higgs pair production $h_1^+ h_1^-$ also contributes to the final state when one of the charged Higgs in the pair production decays to ZW^\pm and the other decays to tb which is one of the substantial decay channels especially for BP2 and BP3 with $\text{Br}(h_1^\pm \rightarrow tb) \gtrsim 40\%$ (see Table 4). The aforementioned final state can be obtained even when both the charged Higgs bosons decay to ZW^\pm , but this time one of the Z boson decays to $b\bar{b}$. Table 7 gives the number of events in benchmark points for the signal and the SM backgrounds at an integrated luminosity of 1000 fb^{-1} at the LHC with $E_{cm} = 14 \text{ TeV}$. As expected $h_1^\pm \phi$ contributes most. In the case of BP2 the contribution is much smaller than the $\text{Br}(h_2 \rightarrow b\bar{b}) \sim 1\%$ (see Table 2). The next largest contribution comes from the h_1^\pm pair production as explained above. The signal significances can be read from Table 7 and again BP1 is the first to give the 5σ significance at an integrated luminosity of $\sim 100 \text{ fb}^{-1}$. For BP2 it takes around 1000 fb^{-1} of integrated luminosity to reach the 5σ significance.

From Table 4 we can see that for BP1 and BP4 the charged Higgs also decays to $\tau\nu$

Production processes	Benchmark Points				Backgrounds			
	BP1	BP2	BP3	BP4	$t\bar{t}$	$t\bar{t}Z$	$t\bar{t}W$	VV
$h_1^\pm h_1^\mp$	30.07	59.93	54.39	13.34				
$h_1^\pm W^\mp$	30.44	0.00	0.00	0.81				
$h_1^\pm \phi$	410.27	60.29	358.22	278.76	99.25	143.78	69.03	118.75
$h_1^\pm t$	4.64	1.57	0.00	0.00				
$h_1^\pm tb$	9.66	3.08	0.00	0.00				
Total	485.08	124.87	412.61	292.91	430.81			
Significance	15.68	5.12	14.21	10.89				

Table 7: Number of events after the selection cuts for $\geq 3\ell (|M_{\ell\ell} - M_Z| \leq 5\text{GeV}) + (\geq 2b - \text{jets}) + \cancel{p}_T \geq 30\text{ GeV}$ final state for the benchmark points and backgrounds at an integrated luminosity of 1000 fb^{-1} at the LHC with $E_{cm} = 14\text{ TeV}$. Here $h_1^\pm \phi$ includes contributions from both $h_1^\pm h_2$ and $h_1^\pm A_1$.

significantly. Also W^\pm can decay to $\tau\nu$, and thus $h_1^\pm W^\mp$ and the other production processes contribute to the single tau final states. In Table 8 we have considered $\geq 3\ell (|M_{\ell\ell} - M_Z| \leq 5\text{GeV}) + (\geq 1\tau - \text{jet}) + (\cancel{p}_T \geq 30\text{ GeV})$. The demand of an extra tau-jet on top of three leptons (e and/or μ) reduces the backgrounds substantially. Here by τ -jet we considered the hadronic decay of the τ with at least one charged track within $\Delta R \leq 0.1$ of the candidate τ -jet [55]. Table 8 presents the corresponding numbers at 1000 fb^{-1} of integrated luminosity at the 14 TeV LHC. We can see that except BP3 all the other benchmark points give $> 5\sigma$. The earliest discovery reach is for BP1 and it takes around 146 fb^{-1} of integrated luminosity.

One can also look for $\geq 3\ell + (\geq 2\tau - \text{jet})$, where the tau pair is coming from the decays of the neutral Higgses (h_2, A_1). We have analysed this particular final state as well and it turns out to require $\gtrsim 1000\text{ fb}^{-1}$ integrated luminosity for a discovery.

5.2 4ℓ final states

We explore the possibility where the associated particle to the light charged Higgs boson h_1^\pm can contribute to the leptonic final states. Thus we expect all the production processes to contribute in $\geq 4\ell$ the final states. The number of events for $\geq 4\ell + (\cancel{p}_T \geq 30\text{ GeV})$ at an integrated luminosity of 1000 fb^{-1} at the LHC with $E_{cm} = 14\text{ TeV}$ are listed in Table 9. $t\bar{t}$ and VV still contribute as dominant backgrounds. At 1000 fb^{-1} BP1 and BP2 give 11σ and 9σ , respectively, whereas BP3 and BP4 give nearly 5σ significance.

Production processes	Benchmark Points				Backgrounds			
	BP1	BP2	BP3	BP4	$t\bar{t}$	$t\bar{t}Z$	$t\bar{t}W$	VV
$h_1^+ h_1^-$	221.00	36.10	50.52	225.58				
$h_1^\pm W^\mp$	55.47	0.00	0.00	1.91				
$h_1^\pm \phi$	37.72	70.18	25.38	19.00	0.00	25.06	0.00	237.51
$h_1^\pm t$	3.80	1.07	0.00	0.00				
$h_1^\pm tb$	2.96	0.05	0.00	0.00				
Total	320.96	108.41	75.89	246.50	262.57			
Significance	13.08	5.53	4.13	10.93				

Table 8: Number of events for $\geq 3\ell$ ($|M_{\ell\ell} - M_Z| \leq 5\text{GeV}$) + ($\geq 1\tau - jet$) + ($\cancel{p}_T \geq 30\text{ GeV}$) final state for the benchmark points and backgrounds at an integrated luminosity of 1000 fb^{-1} at the LHC with $E_{cm} = 14\text{ TeV}$. Here $h_1^\pm \phi$ includes contributions from both $h_1^\pm h_2$ and $h_1^\pm A_1$.

Production processes	Benchmark Points				Backgrounds			
	BP1	BP2	BP3	BP4	$t\bar{t}$	$t\bar{t}Z$	$t\bar{t}W$	VV
$h_1^+ h_1^-$	344.82	152.82	223.34	243.57				
$h_1^\pm W^\mp$	283.65	0.00	0.00	12.70				
$h_1^\pm \phi$	85.73	407.63	41.92	27.01	1191.04	651.62	11.5	1425.03
$h_1^\pm t$	14.80	4.54	0.00	0.00				
$h_1^\pm tb$	10.00	3.17	0.00	0.00				
Total	739.00	568.15	265.26	283.28	3279.19			
Significance	11.30	9.04	4.46	4.75				

Table 9: Number of events after the selection cuts for $\geq 4\ell$ + ($\cancel{p}_T \geq 30\text{ GeV}$) final states for the benchmark points and backgrounds at an integrated luminosity of 1000 fb^{-1} at the LHC with $E_{cm} = 14\text{ TeV}$. Here $h_1^\pm \phi$ includes contributions from both $h_1^\pm h_2$ and $h_1^\pm A_1$.

5.3 5ℓ final states

If both the charged Higgses in the pair production decay to ZW^\pm , then we can get 5ℓ and 6ℓ final states depending on the leptonic decays of the Z and W^\pm . Associated neutral Higgs production $h_1^\pm \phi$ can also contribute to 5ℓ final states if the neutral Higgses can decay in the leptonic modes. In Table 10 we present the numbers of events for the $\geq 5\ell$ + ($\cancel{p}_T \geq 30\text{ GeV}$) final state. We see that due to large $\text{Br}(h_2 \rightarrow ZZ) \sim 44\%$, $h_1^\pm \phi$ contributes more to 5ℓ final state. Thus BP2 makes to $\gtrsim 9\sigma$ at 1000 fb^{-1} and BP1 crosses 5σ in the signal significance.

In addition, we have analysed the final state with two more jets ($\geq 5\ell + (2 - jet) + (\cancel{p}_T \geq$

30 GeV)) which comes from the hadronic decay of the second W^\pm of the second charged Higgs in the case of charged Higgs pair production. In this case only charged Higgs pair production contributes to the final state. Although this case is almost background free, the number of signal events is also quite small. Thus only for BP2 it makes to $\sim 5\sigma$ even at 1000 fb^{-1} and for the rest of the benchmark points it either cross 3σ or approach to 3σ . When the second W^\pm also decays leptonically we get $6\ell + \cancel{p}_T$ in the final state. This final state is absolutely background free but with low signal event counts, and only BP1 and BP2 can cross 2σ signal significance.

Production processes	Benchmark Points				Backgrounds			
	BP1	BP2	BP3	BP4	$t\bar{t}$	$t\bar{t}Z$	$t\bar{t}W$	VV
$h_1^+ h_1^-$	22.78	14.62	21.48	13.19				
$h_1^\pm W^\mp$	0.23	0.00	0.00	0.00				
$h_1^\pm \phi$	11.30	75.04	3.39	2.97	0.00	2.64	1.64	0.00
$h_1^\pm t$	0.03	0.00	0.00	0.00				
$h_1^\pm tb$	0.04	0.004	0.00	0.00				
Total	34.38	89.67	24.87	16.16	4.28			
Significance	5.52	9.25	4.61	3.57				

Table 10: Number of events after the selection cuts for $\geq 5\ell + (\cancel{p}_T \geq 30 \text{ GeV})$ final state for the benchmark points and backgrounds at an integrated luminosity of 1000 fb^{-1} at the LHC with $E_{cm} = 14 \text{ TeV}$. Here $h_1^\pm \phi$ includes contributions from both $h_1^\pm h_2$ and $h_1^\pm A_1$.

6. Mass distributions

When the charged Higgs h_1^\pm decays to ZW^\pm , it is possible to reconstruct the mass of the charged Higgs via constructing the invariant mass of di-lepton and di-jet; where the di-lepton comes from Z and the di-jet from the W^\pm . If we demand that the associated particle (W^\pm, h_2, A_1 or h_1^\pm) provides the other lepton such that the final state has $\geq 3\ell$, it can kill the backgrounds substantially. In Figure 7 (left) we present the invariant mass distribution of $M_{\ell\ell jj}$ for BP1 with $(\geq 3\ell) + (\cancel{p}_T \geq 30 \text{ GeV})$ final state, where $|M_{\ell\ell} - M_Z| \leq 5 \text{ GeV}$ and $|M_{jj} - M_{W^\pm}| \leq 10 \text{ GeV}$ cuts are applied to ensure the reconstruction of Z and W^\pm , respectively. Whenever the Z and W^\pm come from the decay of the light charged Higgs h_1^\pm , i.e. with the right combination, we get the invariant mass peaked around $M_{h_1^\pm}$. The wrong combination will give us the threshold of the production process (in case of $h_1^\pm W^\mp$) which can be seen as the edge after the hump in the distribution. In Figure 7 (right) we present the invariant mass distribution of $M_{\ell\ell jj}$ for BP1 with $(\geq 3\ell) + \geq 2j + (\cancel{p}_T \geq 30$

GeV) final state. Although the number of events decreases compared to the previous one, the end edge distribution is much clearer now. In case of $(\geq 3\ell)+ \geq 2j + (p_T \geq 30 \text{ GeV})$ (Figure 7 (left)), Higgs mass peak around 183 GeV gets 7.6σ signal significance over SM backgrounds whereas for $(\geq 3\ell)+ \geq 2j + (p_T \geq 30 \text{ GeV})$ (Figure 7 (left)), the significance is around 7.3σ .

In particular, Figure 8 shows the corresponding contribution of $h_1^\pm W^\mp$ production channel for BP1 and BP4. Clearly we can see the charged Higgs mass peak around 180 GeV but there is an edge at the end of the invariant mass distribution, which is the artifact of the s-channel threshold i.e., h_2 or A_1 . In other words, the edge at different mass values for different benchmark points carries hidden information about the heavier Higgs bosons. For BP1 the edge is around $\gtrsim 500 \text{ GeV}$, whereas for BP4 it comes around $\gtrsim 300 \text{ GeV}$ (see Figure 8). In the case of BP1 the dominant contribution comes from A_1 as it is most doublet type (see Table 1) neutral Higgs so that it dominantly couples to the quarks. In the case of BP4, it is the h_2 which has relatively more doublet component, so dominantly contribute in the production process.

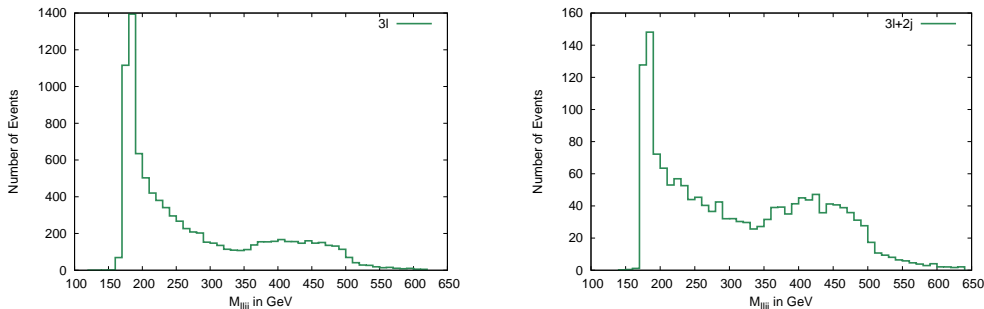


Figure 7: The $\ell\ell jj$ invariant mass distributions coming from the signal for BP1 for $\geq 3\ell + (p_T \geq 30 \text{ GeV})$ (left) and $\geq 3\ell + 2j + (p_T \geq 30 \text{ GeV})$ (right) final states at an integrated luminosity of 1000 fb^{-1} .

Figure 7 shows that all the dominant production processes give a peak around the right charged Higgs mass. The demand of ≥ 3 lepton final state makes the distribution almost background free. So these multi-lepton final states not only probe $Z - W^\pm - h_i^\mp$ coupling but also get the mass information of the light charged Higgs as well as the heavier neutral Higgs boson. The non-standard decays of charged Higgs opens a new era of light charged Higgs phenomenology and the multi-lepton final states along with the mass reconstruction could be a very handy tools to probe these decays.

Above mentioned multi-lepton signatures carry the information of the charged Higgs

decay to ZW^\pm and the discovery of such a final state can provide the information about the presence of higher multiplet structure in the Higgs sector. Besides the production channels containing non supersymmetric particles, the charged Higgs productions via supersymmetric decays are quite interesting and some studies have already been performed in the context of MSSM [56]. We are also working on similar analysis which would also provide some information about the structure of the Higgs sector as well as the supersymmetric electroweak gauginos and the third generation squark mass spectrum [57].

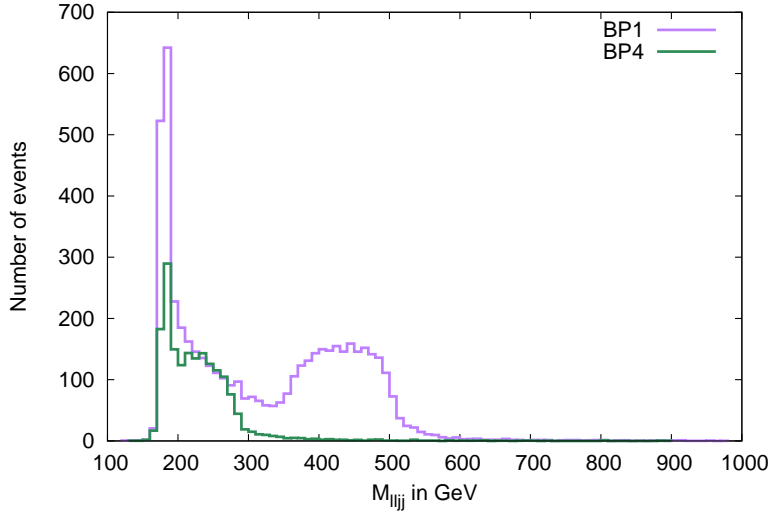


Figure 8: $h_1^\pm W^\pm$ contribution to $\ell\ell jj$ invariant mass distribution for $\geq 3\ell + (p_T \geq 30 \text{ GeV})$ final state for BP1 and BP4 at an integrated luminosity of 1000 fb^{-1} . In BP4 number of events are multiplied by 5.

7. Conclusions

In this article we have studied the multi-lepton signatures of triplet like charged Higgs at the LHC in the $Y = 0$ triplet extended supersymmetric model (TESSM). First of all, to understand the triplet impact on charged Higgs sector of the model we performed a parameter scan where we calculated the lightest neutral Higgs boson mass numerically at one-loop level and we collected points satisfying the direct search constraints along with the measured Higgs mass. We have shown that for many points, the lightest charged Higgs is non-degenerate in mass with CP odd and heavy CP even Higgs bosons. We observed that the presence of the non-degeneracy allows on-shell CP odd or CP even Higgs boson to

decay into a charged Higgs and W^\pm ($h_2(A_1) \rightarrow h_1^\pm W^\mp$) which is not kinematically possible in the case of the MSSM.

In addition to the non-degeneracy, the existence of a triplet with non-zero vev provides the tree level $h_i^\pm ZW^\mp$ coupling that is only induced at loop order in the case of two Higgs doublet models. This vertex can be used to discriminate the triplet nature among the other structures in the Higgs sector. For this purpose we have investigated the strength of the coupling for different scenarios with the charged Higgs mass $m_{h_1^\pm} \leq 200$ GeV and shown that for triplet like charged Higgs, the ZW^\pm decay channel can be as substantial as tb and $\tau\nu_\tau$. In particular, we have shown that when the lightest charged Higgs comprises 99% triplet nature the ZW^\pm channel remains the most dominant channel even after tb channel is kinematically open.

Besides the decay channels, we have investigated the production channels for the triplet like charged Higgs at the LHC to distinguish the signatures of the model from the ones in the two Higgs doublet models. Due to the lack of triplet-SM fermion coupling, the production channel through the top decay $t \rightarrow bh_1^\pm$ or the associated production with a top quark through the gg/gb fusions are no longer the dominant ones for the triplet like charged Higgs. This is why we have explored alternative production channels such as charged Higgs pair production, associated production with massive gauge bosons (W^\pm, Z) and neutral Higgs bosons. We have also considered the charged Higgs production through vector boson fusion that is possible with the presence of $h_i^\pm ZW^\mp$ coupling. Then we discussed the possibility of having triplet like neutral Higgs boson along with the charged ones where the production mechanisms through the neutral Higgs propagators are expected to be suppressed.

To determine the dominant production channels we have considered four benchmark points where we performed PYTHIA level simulation using FastJet jet information at the LHC with 14 TeV. We analysed the signal in $3l, 4l, 5l$ final states with τ and b-jets. It is possible to reduce the SM background substantially by using the different selection cuts for the multi-lepton and jets and the earliest discovery hints can be obtained with $\gtrsim 72$ fb $^{-1}$ integrated luminosity. We have also presented the invariant mass distribution M_{lljj} for $(\geq 3l) + (\cancel{p}_T \geq 30 \text{ GeV})$ and $(\geq 3l) + (\geq 2j) + (\cancel{p}_T \geq 30 \text{ GeV})$ and shown that in addition to the charged Higgs mass peak, an edge that carries information about heavy intermediate neutral Higgs bosons emerges at the end of the mass distribution.

Acknowledgments: The authors gratefully acknowledge support from the Academy of Finland (Project No. 137960). The work of ASK is also supported by the Finnish Cultural Foundation. PB also thanks INFN, Lecce, for the support at the finishing part of the project.

References

- [1] S. Chatrchyan *et al.* [CMS Collaboration], Phys. Lett. B **716** (2012) 30 [arXiv:1207.7235 [hep-ex]].
- [2] G. Aad *et al.* [ATLAS Collaboration], Phys. Lett. B **716** (2012) 1 [arXiv:1207.7214 [hep-ex]].
- [3] S. Chatrchyan *et al.* [CMS Collaboration], Phys. Rev. D **89** (2014) 092007 [arXiv:1312.5353 [hep-ex]].
- [4] [ATLAS Collaboration], ATLAS-CONF-2013-013.
- [5] S. Chatrchyan *et al.* [CMS Collaboration], JHEP **1401** (2014) 096 [arXiv:1312.1129 [hep-ex]].
- [6] [ATLAS Collaboration], ATLAS-CONF-2013-030.
- [7] S. Chatrchyan *et al.* [CMS Collaboration], Phys. Rev. D **89** (2014) 012003 [arXiv:1310.3687 [hep-ex]].
- [8] [ATLAS Collaboration], ATLAS-CONF-2012-161.
- [9] S. Chatrchyan *et al.* [CMS Collaboration], JHEP **1405** (2014) 104 [arXiv:1401.5041 [hep-ex]].
- [10] The ATLAS collaboration, ATLAS-CONF-2013-108.
- [11] [CMS Collaboration], CMS-PAS-HIG-13-001.
- [12] [ATLAS Collaboration], ATLAS-CONF-2013-012.
- [13] G. C. Branco, P. M. Ferreira, L. Lavoura, M. N. Rebelo, M. Sher and J. P. Silva, Phys. Rept. **516** (2012) 1 [arXiv:1106.0034 [hep-ph]].
- [14] A. Djouadi, Phys. Rept. **459** (2008) 1 [hep-ph/0503173].
- [15] A. Djouadi, J. Kalinowski and P. M. Zerwas, Z. Phys. C **70** (1996) 435 [hep-ph/9511342].
- [16] S. Dittmaier, C. Mariotti, G. Passarino, R. Tanaka, S. Alekhin, J. Alwall and E. A. Bagnaschi *et al.*, arXiv:1201.3084 [hep-ph].
- [17] E. L. Berger, T. Han, J. Jiang and T. Plehn, Phys. Rev. D **71** (2005) 115012 [hep-ph/0312286].
- [18] J. F. Gunion, H. E. Haber, F. E. Paige, W. K. Tung and S. S. D. Willenbrock, Nucl. Phys. B **294** (1987) 621.
- [19] J. L. Diaz-Cruz and O. A. Sampayo, Phys. Rev. D **50** (1994) 6820.
- [20] V. D. Barger, R. J. N. Phillips and D. P. Roy, Phys. Lett. B **324** (1994) 236 [hep-ph/9311372].
- [21] T. Plehn, Phys. Rev. D **67** (2003) 014018 [hep-ph/0206121].
- [22] C. Weydert, S. Frixione, M. Herquet, M. Klasen, E. Laenen, T. Plehn, G. Stavenga and C. D. White, Eur. Phys. J. C **67** (2010) 617 [arXiv:0912.3430 [hep-ph]].

- [23] J. F. Gunion, G. L. Kane and J. Wudka, Nucl. Phys. B **299** (1988) 231.
- [24] A. Mendez and A. Pomarol, Nucl. Phys. B **349** (1991) 369.
- [25] M. Capdequi Peyranere, H. E. Haber and P. Irulegui, Phys. Rev. D **44** (1991) 191.
- [26] S. Kanemura, Phys. Rev. D **61** (2000) 095001 [hep-ph/9710237].
- [27] M. Carena, S. Gori, N. R. Shah and C. E. M. Wagner, JHEP **1203** (2012) 014 [arXiv:1112.3336 [hep-ph]].
- [28] M. W. Cahill-Rowley, J. L. Hewett, A. Ismail and T. G. Rizzo, Phys. Rev. D **86** (2012) 075015 [arXiv:1206.5800 [hep-ph]].
- [29] M. W. Cahill-Rowley, J. L. Hewett, A. Ismail and T. G. Rizzo, Phys. Rev. D **88** (2013) 3, 035002 [arXiv:1211.1981 [hep-ph]].
- [30] P. Bandyopadhyay, K. Huitu and A. Sabanci, arXiv:1306.4530 [hep-ph].
- [31] A. Delgado, G. Nardini and M. Quiros, arXiv:1303.0800 [hep-ph].
- [32] P. Bandyopadhyay, S. Di Chiara, K. Huitu and A. S. Keceli, arXiv:1407.4836 [hep-ph].
- [33] S. D. Chiara and K. Hsieh, Phys. Rev. D **78** (2008) 055016.
- [34] A. Delgado, G. Nardini and M. Quiros, Phys. Rev. D **86** (2012) 115010 [arXiv:1207.6596 [hep-ph]].
- [35] C. Arina, V. Martin-Lozano and G. Nardini, JHEP **1408** (2014) 015 [arXiv:1403.6434 [hep-ph]].
- [36] E. Barradas-Guevara, O. Felix-Beltran and A. Rosado, Phys. Rev. D **71** (2005) 073004 [hep-ph/0408196].
- [37] J. L. Diaz-Cruz, J. Hernandez-Sanchez, S. Moretti and A. Rosado, Phys. Rev. D **77** (2008) 035007 [arXiv:0710.4169 [hep-ph]].
- [38] ATLAS-CONF-2013-007, ATLAS-CONF-2014-050, CMS PAS HIG-14-020, CMS PAS HIG-13-026.
- [39] P. Bandyopadhyay and K. Huitu, JHEP **1311** (2013) 058 [arXiv:1106.5108 [hep-ph]].
- [40] J. Beringer *et al.* [Particle Data Group Collaboration], Phys. Rev. D **86** (2012) 010001.
- [41] S. R. Coleman and E. J. Weinberg, Phys. Rev. D **7** (1973) 1888.
- [42] S. Chatrchyan *et al.* [CMS Collaboration], Phys. Rev. D **89** (2014) 092007 [arXiv:1312.5353 [hep-ex]]. S. Chatrchyan *et al.* [CMS Collaboration], JHEP **1401** (2014) 096 [arXiv:1312.1129 [hep-ex]].
- [43] The ATLAS collaboration, ATLAS-CONF-2014-009.
- [44] S. Chatrchyan *et al.* [CMS Collaboration], Phys. Rev. D **89** (2014) 092007 [arXiv:1312.5353 [hep-ex]],

- [45] The ATLAS collaboration, ATLAS-CONF-2014-009, ATLAS-COM-CONF-2014-013.
- [46] F. Staub, *Comput. Phys. Commun.* **181** (2010) 1077 [arXiv:0909.2863 [hep-ph]].
- [47] F. Staub, T. Ohl, W. Porod and C. Speckner, *Comput. Phys. Commun.* **183** (2012) 2165 [arXiv:1109.5147 [hep-ph]].
- [48] A. Pukhov, hep-ph/0412191. A. Belyaev, N. D. Christensen and A. Pukhov, *Comput. Phys. Commun.* **184** (2013) 1729 [arXiv:1207.6082 [hep-ph]].
- [49] M. Cacciari, G. P. Salam and G. Soyez, *Eur. Phys. J. C* **72** (2012) 1896 [arXiv:1111.6097 [hep-ph]].
- [50] A. Arbey, M. Battaglia, A. Djouadi, F. Mahmoudi and J. Quevillon, *Phys. Lett. B* **708** (2012) 162 [arXiv:1112.3028 [hep-ph]].
- [51] P. Skands *et al.*, *JHEP* **0407**, 036 (2004) [arXiv:hep-ph/0311123];
see also <http://home.fnal.gov/skands/slha/>
- [52] T. Sjostrand, L. Lonnblad and S. Mrenna, [arXiv:hep-ph/0108264].
- [53] H. L. Lai *et al.* [CTEQ Collaboration], *Eur. Phys. J. C* **12**, 375 (2000) [arXiv:hep-ph/9903282].
- [54] J. Pumplin, D. R. Stump, J. Huston, H. L. Lai, P. Nadolsky and W. K. Tung, *JHEP* **0207**, 012 (2002) [arXiv:hep-ph/0201195].
- [55] G. Bagliesi, arXiv:0707.0928 [hep-ex]. G. L. Bayatian *et al.* [CMS Collaboration], *J. Phys. G* **34** (2007) 995.
- [56] P. Bandyopadhyay, *JHEP* **1108** (2011) 016 [arXiv:1008.3339 [hep-ph]]. P. Bandyopadhyay, *JHEP* **0907** (2009) 102 [arXiv:0811.2537 [hep-ph]]. P. Bandyopadhyay, A. Datta and B. Mukhopadhyaya, *Phys. Lett. B* **670** (2008) 5 [arXiv:0806.2367 [hep-ph]].
- [57] P. Bandyopadhyay, K. Huitu and Asli Sabancı Keçeli (in preparation)